

# Oxidation Resistance of Turbine Blades Made of ŽS6K Superalloy after Aluminizing by Low-Activity CVD and VPA Methods

M. Zagula-Yavorska, P. Kocurek, M. Pytel, and J. Sieniawski

(Submitted May 15, 2015; in revised form March 10, 2016; published online April 5, 2016)

Two aluminide layers (additive and interdiffusion) were deposited on a turbine blade made of ŽS6K superalloy by means of VPA and CVD methods. The additive and interdiffusion layers obtained by the VPA method consist of the NiAl phase and some carbides, while the additive layer deposited by the CVD method consists of the NiAl phase only. The residual stresses in the aluminide coating at the lock, suction side, and pressure side of the blade were tensile. The aluminide coating deposited by the CVD method has an oxidation resistance about 7 times better than that deposited by the VPA method.  $\text{Al}_2\text{O}_3 + \text{HfO}_2 + \text{NiAl}_2\text{O}_4$  phases were revealed on the surface of the aluminide coating deposited by the VPA method after 240 h oxidation.  $\text{Al}_2\text{O}_3 + \text{TiO}_2$  oxides were found on the surface of the aluminide coating deposited by the CVD method after 240 h oxidation. Increasing the time of oxidation from 240 to 720 h led to the formation of the NiO oxide on the surface of the coating deposited by the VPA method.  $\text{Al}_2\text{O}_3$  oxide is still visible on the surface of the coating deposited by the CVD method. The residual stresses in the aluminide coating after 30 cycles of oxidation at the lock, suction side and pressure side of the turbine blade are compressive.

**Keywords** aerospace, coatings and paints, oxidation

## 1. Introduction

The increasing efficiency of advanced turbine engines requires higher operation temperatures for more complete combustion of fuels. At the high working temperature above 1000 °C, surface oxidation becomes the life limiting factor (Ref 1). Diffusive nickel aluminide coatings are widely used to protect nickel-based superalloys against oxidation (Ref 2). Aluminide coatings rely on formation of the  $\beta$ -NiAl phase on the surface of the alloys. Three major processes, by which aluminide can be deposited include: pack cementation, vapor phase aluminizing (VPA) and chemical vapor deposition (CVD). One of the steps, which is common in these three processes, is the generation of vapors containing aluminum or the other metallic constituents of the coatings. The vapor phase is transported to the chamber and reacts with the alloy which forms the aluminide coating. In the pack process, the component is embedded in, and therefore in intimate contact with a pack mix in a heated retort (Ref 3). The pack generates the halide vapors. In the vapor phase aluminizing process (VPA), the component to be coated is inside the retort but not in contact with the pack (Al-Cr alloy and  $\text{Al}_2\text{O}_3$  filler). The halide vapors are plumbed on to the accessible internal and external surfaces of the component. In the CVD process, the halide vapor sources are external in individual generators and vapors are plumbed on

to the component held inside a reactor in a heated retort (Ref 4, 5). The aluminum activity plays a critical role in determining the predominant diffusing species. Depending on the content of aluminum in the pack and the processing temperature, the coating process is termed a “low-activity” or “high activity” one. When the aluminum activity is low and the temperature is above 1000 °C, the predominant diffusing species is nickel, which diffuses out of the alloy, producing an ‘outward diffusion’ coating. If the aluminum activity is high and the temperature is below 950 °C, aluminum diffuses inwards, resulting in an “inward diffusion” coating. Aluminum is also the predominant diffusing species in the  $\text{Ni}_2\text{Al}_3$  phase. In the low-activity process, nickel is a predominant diffusing species, which diffuses outwards and combines with aluminum to form the external NiAl zone. Near the interface, the internal zone, which is also called the interdiffusion zone, loses nickel. Many of the alloying constituents of the alloy have very low solubility in the NiAl phase formed in the inner zone. The total coating thickness includes both the external and the interdiffusion zones. Both of the zones consist of the NiAl phase, but only in the interdiffusion zone carbides are formed. Aluminum is the predominant diffusing species in the high-activity coating process. The consequence of the higher inward diffusion of aluminum to nickel is that the original surface becomes the external surface of the coating (Ref 6).

Aluminum in the coating combines with the oxygen which forms the protective  $\alpha$ - $\text{Al}_2\text{O}_3$  oxide. When the oxide cracks and spalls due to thermal cycling, additional aluminum from the coating diffuses to the surface to reform the oxide. When the aluminum content in the coatings drops to about 4 or 5% at., the  $\alpha$ - $\text{Al}_2\text{O}_3$  oxide can no longer be formed and rapid oxidation occurs (Ref 7).

Watanabe et al. (Ref 8) reported that the residual stress in the aluminide coatings caused by cooling from the manufacturing temperature facilitates, yielding of the coatings. It does so by interacting with the stress in the aluminide coating caused by

M. Zagula-Yavorska, P. Kocurek, M. Pytel, and J. Sieniawski, Department of Materials Science, Rzeszow University of Technology, W. Pola 2 Str., 35-959 Rzeszow, Poland. Contact e-mail: yavorska@prz.edu.pl.

the thermal expansion misfit with the thermally grown oxide. It causes an acceleration of the degradation of coated elements at high temperature. Therefore, there is a strong need of a thorough investigation of the correlation between residual stresses and degradation of coated elements.

This paper presents the results of the research performed on the aluminide coating deposited by the CVD and VPA methods on the turbine blade made of ŽS6K superalloy. The oxidation behavior of coated turbine blades was evaluated. Moreover, the residual stresses after aluminization and oxidation were investigated.

## 2. Experimental

The nickel-based turbine blades made of ŽS6K superalloy were used as a substrate. The chemical composition of this superalloy is: 0.14 wt.% C, 10.2 wt.% Cr, 5.2 wt.% W, 4.7 wt.% Co, 3.7 wt.% Mo, 5.3 wt.% Al, 2.8 wt.% Ti, 1.5 wt.% Fe, and the balance nickel (Ref 2).

Two kinds of coatings were produced on the turbine blades: namely deposited by the CVD and PVD processes.

The aluminized turbine blades were subjected to the oxidation test at 1100 °C in an air atmosphere for 1000 h. Samples were heated up to 1100 °C, kept at that temperature for 20 h and then cooled down in the air to the room temperature and then weighed with accuracy of 0.0001 g.

The microstructure of the surface of the synthesized coatings was investigated by the scanning electron microscope (SEM) Hitachi S-3400N and the energy dispersive spectroscope (EDS) (Ref 9-11).

Macroscopic residual stresses in as deposited aluminide coatings and after the oxidation test were determined using the Proto I XRD diffractometer. Asymmetric geometry was used to measure  $\omega \sin^2 \psi$  and interplanar spacing determined as a function of  $\psi$  tilt angle of x-rays to determine the strain of the specimen (Ref 12-15).

A mobile x-ray diffraction residual stress analyzer with a horizontal goniometer fixture was used to measure residual stress in the samples. The specimen axis for  $\psi$  tilt is vertical and the arrangement of the diffractometer is based on the Bragg-Bentano focusing principle.

Cobalt x-ray source with a spot diameter of 2 mm was used. X-ray tube operating parameters were 20 kV and 4 mA. Measurements were made by the diffraction of manganese K-alpha radiation from the (311) crystallographic planes with a peak position  $2\Theta = 149^\circ$  with the exposure time of 2 s and number of 20 exposures. The depth of K-alpha radiation was about 10  $\mu\text{m}$ .

Two position scintillation detectors were used to cover positive and negative  $\psi$  angles and the goniometer oscillated over  $3^\circ$  about the main position to obtain better signal-to-noise ratio.

Multiple channel x-ray diffraction data were acquired simultaneously using position sensitive scintillation detectors (PSSD).

Pearson VII peak-fitting algorithm was applied to the intensity data and Lorentz polarization and absorption corrections were used to determine the center of the diffraction peak. For residual stress determination at a given location, the diffraction peak position was determined at seven  $\psi$  tilt angles.

These  $\psi$  values were in the ranges between  $-45.65^\circ$  and  $45.65^\circ$ .

Measurements of the stress by scanning the sample in both orthogonal x and y directions revealed the distribution of the residual stress (Fig. 1).

The diffraction method applied in this research is based on the Bragg's law *i.e.*, lattice spacing is calculated on the basis of the diffraction angle  $2\theta$  and x-ray wavelength. Residual stress in the material causes the shift of the mean positions of diffraction peaks. Usually, it is less than one degree. The magnitude of this shift is proportional to the value of the strain. The residual stress is calculated from the value of this strain. The x-rays can penetrate into material for not more than several  $\mu\text{m}$ . Therefore, it is assumed that the residual stress in the surface is biaxial. It may be described by principle stresses  $\sigma_{11}$  and  $\sigma_{22}$  in the plane of the surface with no stress  $\sigma_{33}$  perpendicular to the free surface. The shear stresses  $\sigma_{13} = \sigma_{31}$  and  $\sigma_{23} = \sigma_{32}$  are then equal to zero (Fig. 2).

The lattice spacing values  $d_{\psi\phi}$  for a given family of lattice planes are determined as a function of  $\sin^2 \psi$ . The slope  $\frac{\partial d_{\psi\phi}}{\partial \sin^2 \psi}$  is determined on the basis of the linear fit to the recorded data

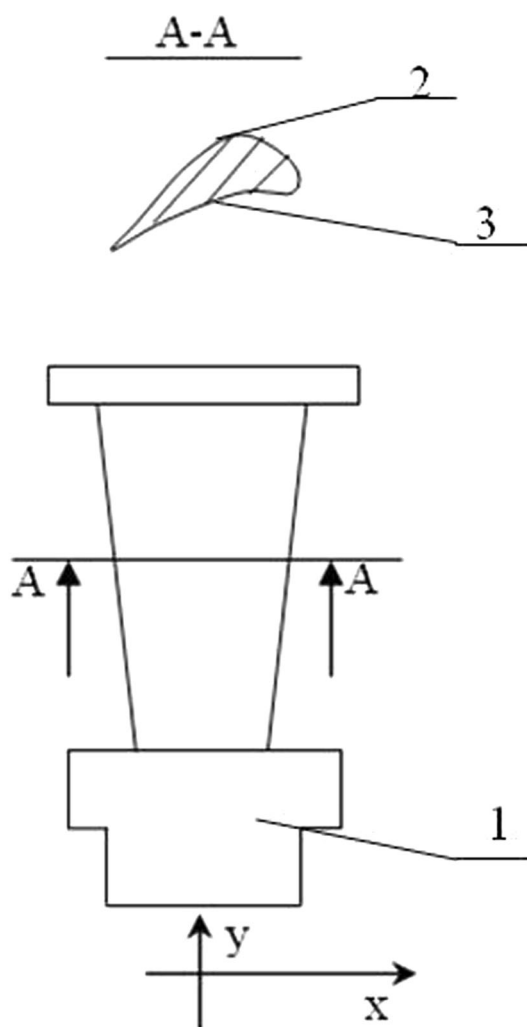


**Fig. 1** A scheme of the turbine blade and places where residual stress measurement was performed: 1—lock of turbine blade, 2—suction side and 3—pressure side

points. Knowing the Young's modulus and Poisson's ratio the residual stress  $\sigma_\phi$  may be calculated according to the equation:

$$\sigma_\phi = \left( \frac{E}{1 + \nu} \right)_{hkl} \frac{1}{d_0} \left( \frac{\partial d_{\phi\Psi}}{\partial \sin^2 \Psi} \right). \quad (\text{Eq 1})$$

One should also know the unstressed lattice spacing  $d_0$  for the analyzed family of lattice planes. As it usually remains unknown,  $d_{\phi 0}$  is applied instead of  $d_0$ . It is determined experimentally at  $\psi = 0$ . This procedure introduces an error which is negligible when compared to other errors.

### 3. Results

The turbine blades made of ŽS6K Ni-based superalloy were aluminized by the vapor deposition method and the low-activity CVD method. The obtained coating covered the turbine blades completely.

The cross-section of the turbine blade after aluminizing by the VPA method is shown in Fig. 3. The microstructural analysis on the cross-section revealed that the coating consisted of two layers: an additive layer and an interdiffusion layer

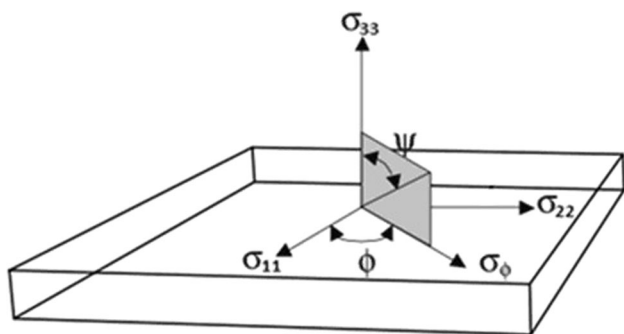


**Fig. 2** The principal axes of the residual stresses  $\sigma$ .  $\Psi$ —angle between the normal to the surface and the normal to the family of diffracting planes  $\{hkl\}$   $M$ ,  $\sigma_\phi$ —stress in the measurement direction,  $\phi$ —angle between the direction of the principal stress  $\sigma_{11}$  and the selected direction of the measurement

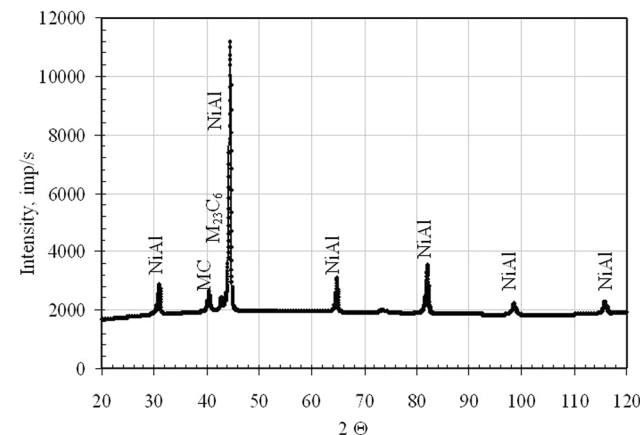
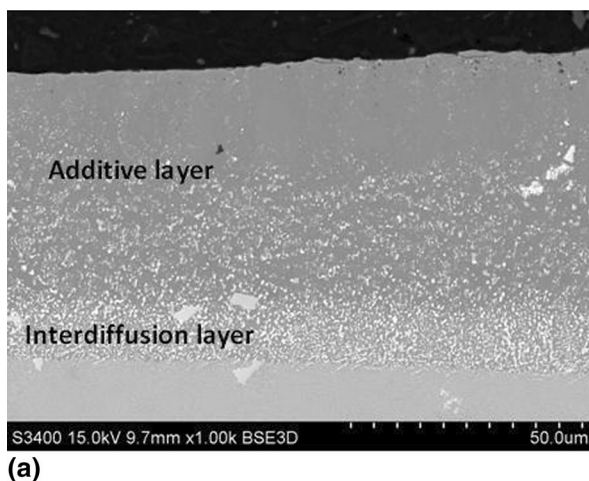


**Fig. 4** XRD pattern of the aluminide coating deposited by the VPA method

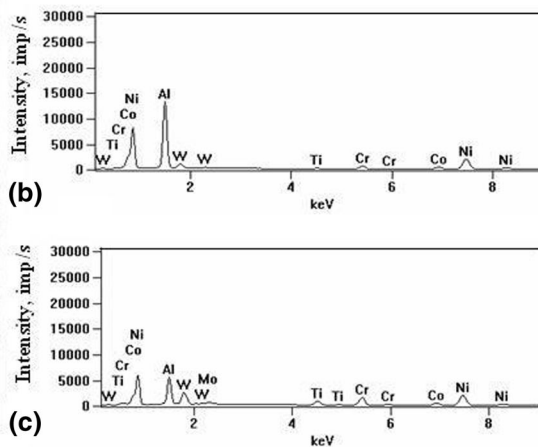


**Fig. 3** The cross-section microstructure of the aluminide coating deposited by the VPA method on the ŽS6K Ni-base superalloy turbine blade (a), EDS spectrum of the additive layer (b), and EDS spectrum of the interdiffusion layer (c)

(Fig. 3a). The total coating thickness is about 65  $\mu\text{m}$ . The EDS analysis results showed that the top additive layer is composed of the  $\beta$ -NiAl phase [50.14 Al-2.87 Cr-0.31 Ti-4.23 Co-42.0 Ni-0.44 W (at.%)] (Fig. 3b). The interdiffusion layer contains precipitates rich in chromium, titanium, tungsten, and molybdenum that were in the substrate (Fig. 3c). The XRD pattern indicates the presence of the NiAl phase and MC,  $M_{23}C_6$  carbides in the coating (Fig. 4).

The microstructure analysis on the cross-section revealed that the CVD coating consists of two layers: an additive layer and interdiffusion layer (Fig. 5a). The total coating thickness is about 34  $\mu\text{m}$ . The EDS analysis results showed that the top additive layer is composed of the  $\beta$ -NiAl phase (39.59 Al-2.15 Cr-5.16 Co-52.92 Ni-0.17W) (at.%) (Fig. 5b). The interdiffusion layer contains precipitates rich in chromium, titanium, tungsten, and molybdenum that diffused from the substrate (Fig. 5c). The XRD pattern indicates the presence of the NiAl phase in the coating (Fig. 6).

It was found that the residual stress in the aluminide coating at the lock, suction side, and pressure side of the turbine blades was tensile (Table 1). Moreover, the values of the residual stress in the x and y directions do not differ significantly (Table 1).

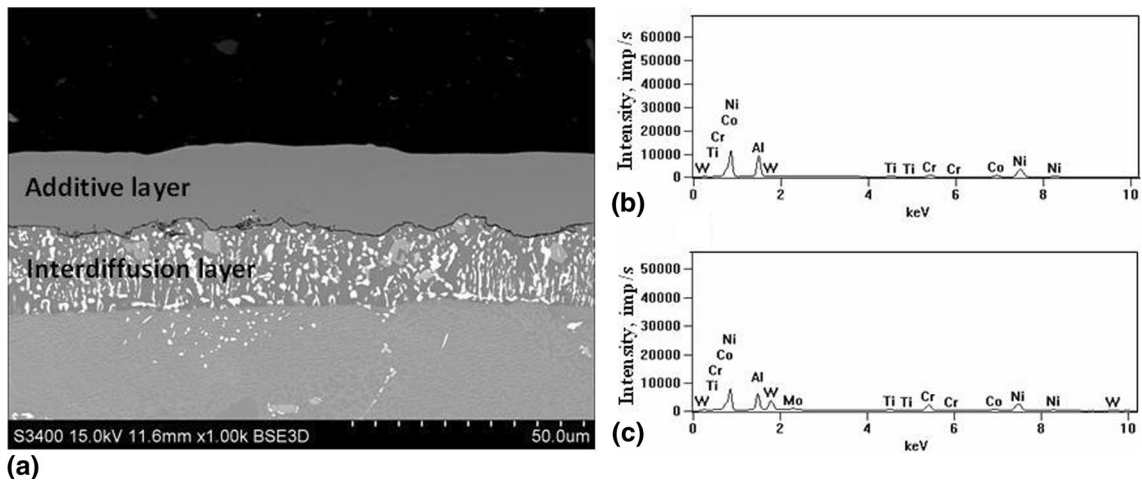


**Fig. 5** The microstructure of the cross-section of the aluminide coating deposited by the low-activity CVD method on the ZS6K Ni-base superalloy turbine blade (a), EDS spectrum of the additive layer (b), and EDS spectrum of the interdiffusion layer (c)

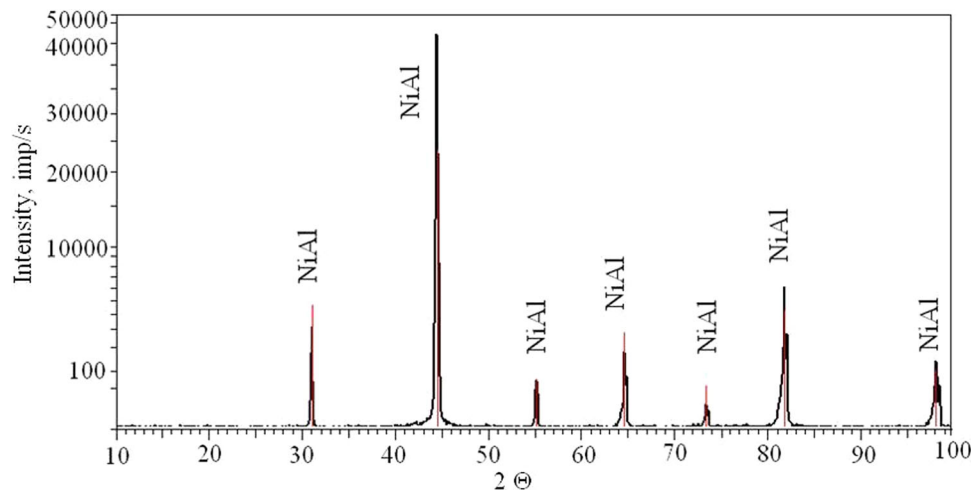


**Fig. 6** XRD pattern of the aluminide coating deposited by the CVD method

**Table 1** XRD residual stress results after the aluminizing process

Coating type	Coating thickness, $\mu\text{m}$	Place of stress measurement on turbine blade	Residual stress, MPa	
			Measurement direction	
			x	y
VPA	65	Lock	$17 \pm 8$	$18 \pm 8$
		Suction side	$28 \pm 4$	$25 \pm 4$
		Pressure side	$30 \pm 7$	$27 \pm 7$
Low-activity CVD	34	Lock	$72 \pm 38$	$109 \pm 32$
		Suction side	$73 \pm 36$	$117 \pm 33$
		Pressure side	$54 \pm 37$	$137 \pm 39$

Mass change curves of aluminide coatings during the cyclic oxidation test are shown in Fig. 7. The aluminide coating deposited by the low-activity CVD method showed better oxidation resistance in comparison to the aluminide coating deposited by the VPA method. The mass change of the ZS6K

turbine blade covered with the aluminide coating deposited by the VPA method is about  $-6.2 \text{ mg/cm}^2$ , while the mass change of the turbine blade covered with the aluminide coating deposited by the low-activity CVD method is about  $0.5 \text{ mg/cm}^2$  after 40 cycles of oxidation in the air atmosphere (Fig. 7).



After 10 cycles of oxidation, the turbine blade aluminized by the VPA process was covered with the green scale that spalled (Fig. 8a). The largest damage was revealed in the pressure side of the turbine blade. After 10 cycles of oxidation, the turbine blade aluminized by the low-activity CVD method was covered with the gray scale (Fig. 8b). The surface analysis did not reveal any fracturing nor cracking in the scale.

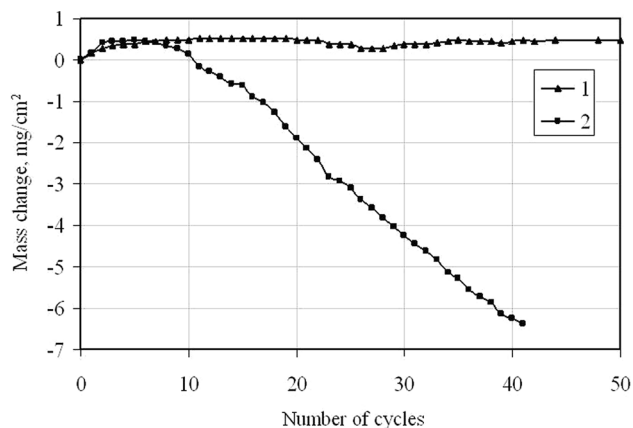


**Fig. 7** Mass change curves of ZS6K superalloy: 1—with the aluminide coating deposited by the low-activity CVD process; 2—with the aluminide coating deposited by the VPA process

The XRD surface analysis results are presented in Table 2.  $\text{Al}_2\text{O}_3 + \text{HfO}_2 + \text{NiAlO}_4$  phases were found in the aluminide coating deposited by the VPA method after 240 h oxidation, while  $\text{Al}_2\text{O}_3 + \text{TiO}_2$  phases were found in the aluminide coating deposited by the CVD method (Table 2).  $\text{NiAl}_2\text{O}_4 +$

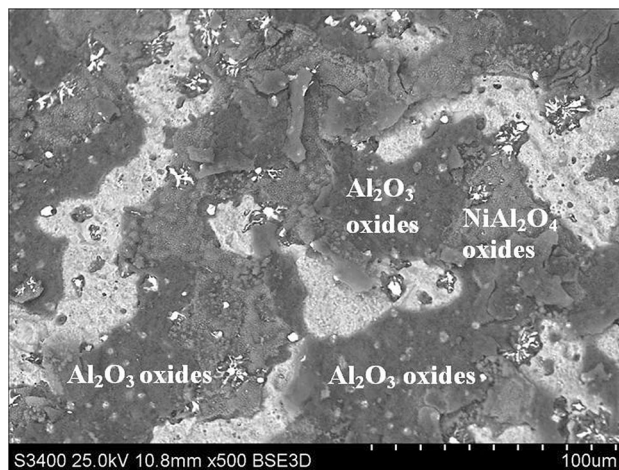


**Fig. 9** SEM micrographs of the scales formed on the aluminide coating deposited by the VPA method after 10 cycles of oxidation at 1100 °C in the air atmosphere

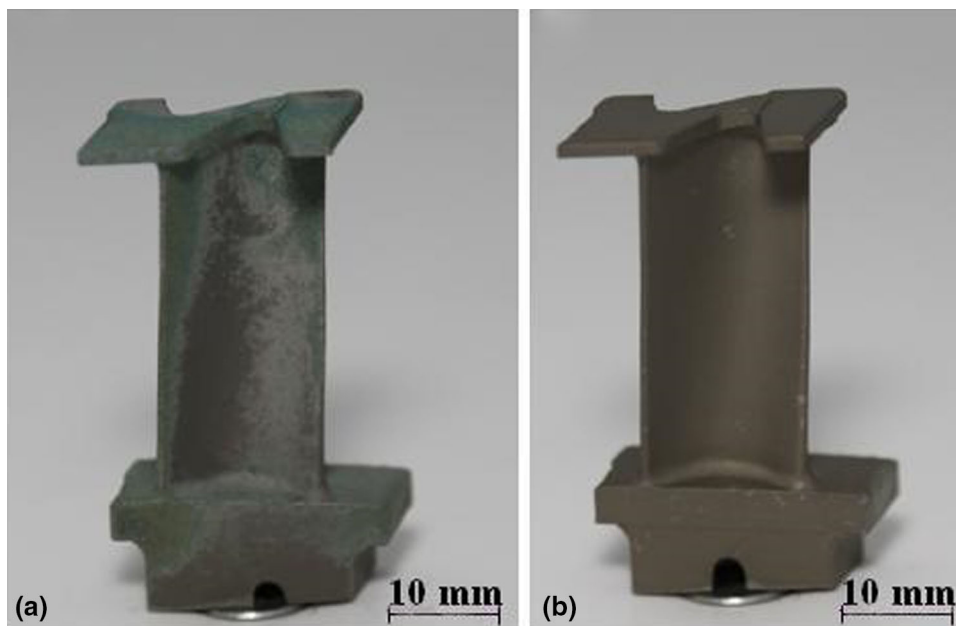


**Fig. 8** Turbine blades: (a) aluminized by the VPA process and (b) aluminized by the CVD process after 10 cycles of oxidation at 1100 °C

**Table 2** XRD surface analysis results of the aluminide coating

Time of oxidation, h	Aluminide coating deposited by the VPA method	Aluminide coating deposited by the CVD method
0	$\text{NiAl} + \text{MC} + \text{M}_{23}\text{C}_6$	$\text{NiAl}$
240	$\text{Al}_2\text{O}_3 + \text{HfO}_2 + \text{NiAl}_2\text{O}_4$	$\text{Al}_2\text{O}_3 + \text{TiO}_2$
720	$\text{NiAl}_2\text{O}_4 + \text{NiO}$	$\text{Al}_2\text{O}_3 + \text{NiO} + \text{HfO}_2$

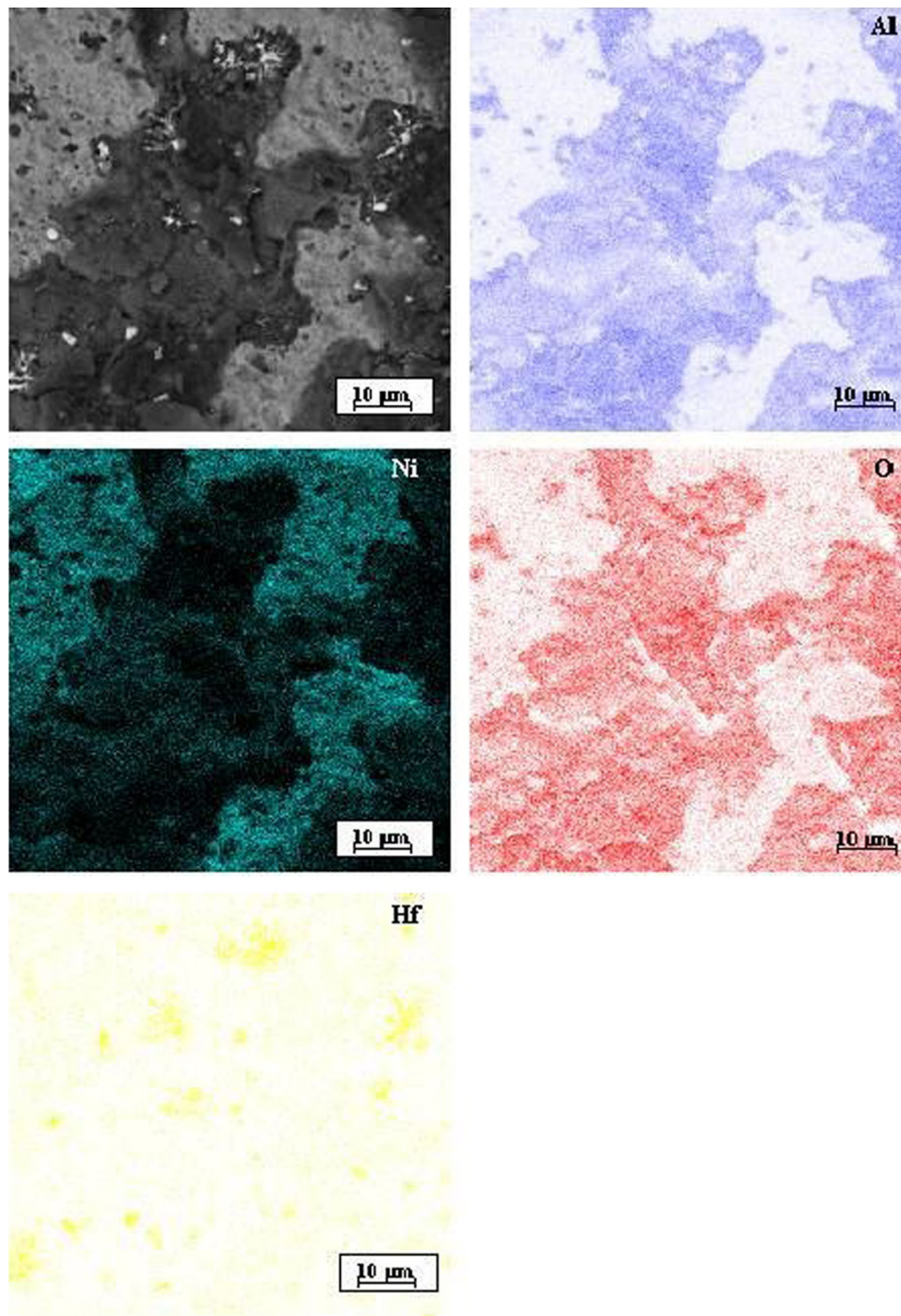


**Fig. 10** The digimap analysis of the aluminide coating deposited by the VPA method after 10 cycles of oxidation at 1100 °C, HfO<sub>2</sub> oxide surrounded by Al<sub>2</sub>O<sub>3</sub> oxide

NiO spinels were formed in the aluminide coating deposited by the VPA method after 720 h oxidation, while Al<sub>2</sub>O<sub>3</sub> oxide still remains in the aluminide coating deposited by the CVD method after 720 h oxidation.

The evident scale spallation was observed on the surface of the aluminide coating deposited by the VPA method after 10 cycles of oxidation. The oxides have nonuniform composition. The chemical composition of the oxides corresponds to NiAl<sub>2</sub>O<sub>4</sub>

[56.04O-29.61Al-1.81Ti-1.53Cr-1.11Co-9.48Ni (at.%) and predominantly Al<sub>2</sub>O<sub>3</sub> oxides [56.57O-38.95Al-0.36Ti-0.68Cr-0.63Co-1.21Ni-1.59Hf (at.%) (Fig. 9). The digimap analysis of the coating after 10-cycles oxidation confirmed the presence of Hf-rich pegs inside Al<sub>2</sub>O<sub>3</sub> oxides (Fig. 10 and 11).

Some scale spallation was observed on the surface of the aluminide coating deposited by the low-activity CVD process after 10 cycles of oxidation. Chemical composition of the scale





**Fig. 11** SEM micrographs of the  $\text{Al}_2\text{O}_3$  and  $\text{HfO}_2$  oxides formed on the aluminide coating deposited by the VPA method after 10 cycles of oxidation at 1100 °C in the air atmosphere

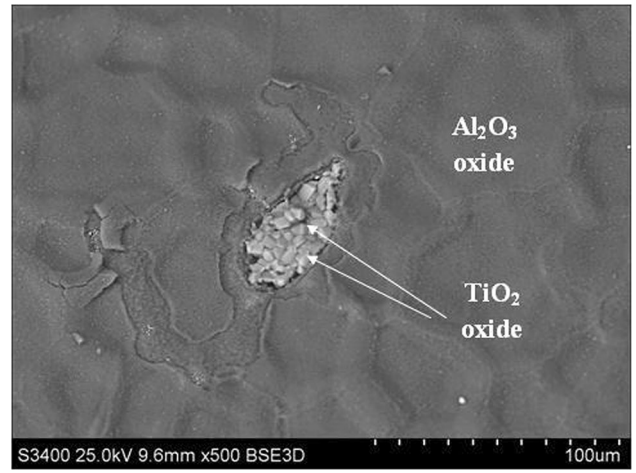


**Fig. 13** SEM micrographs of  $\text{Al}_2\text{O}_3$  and  $\text{TiO}_2$  oxides formed on the aluminide coating deposited by the CVD method after 10 cycles of oxidation at 1100 °C in the air atmosphere

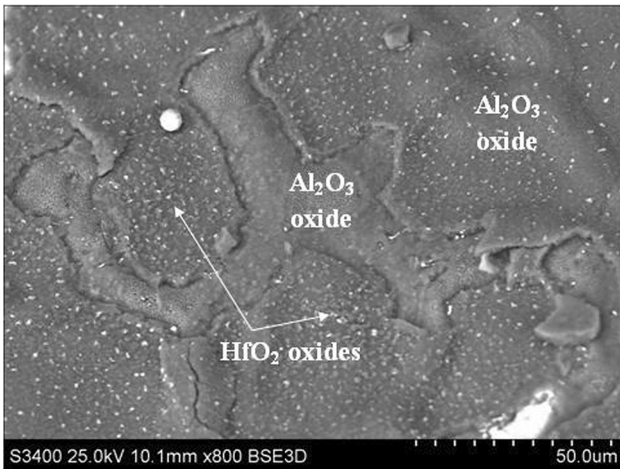


**Fig. 12** SEM micrographs of oxides formed on the aluminide coating deposited by the CVD method after 10 cycles of oxidation at 1100 °C in the air atmosphere

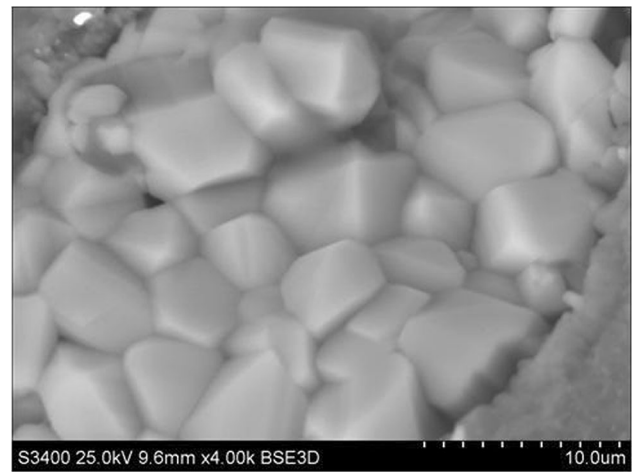


**Fig. 14** SEM micrographs of  $\text{TiO}_2$  oxide formed on the aluminide coating deposited by the CVD method after 10 cycles of oxidation at 1100 °C in the air atmosphere

corresponds to the presence of predominantly  $\text{Al}_2\text{O}_3$  oxide [47.84O-46.42Al-1.14Ti-1.20Cr-0.14Fe-0.88Co-2.37Ni (at.%)] (Fig. 12). The  $\text{TiO}_2$  oxide was in some spots observed in place of alumina oxides (Fig. 13 and 14). After 30 cycles of oxidation, the whole surface of the turbine blade aluminized by the VPA process was covered with a green scale, while a blue scale was observed on the surface of the turbine blade aluminized by the CVD method. A mixture of oxides consisting of  $\text{NiAl}_2\text{O}_4$  and  $\text{NiO}$  oxides was formed (Fig. 15). Some  $\text{HfO}_2$  oxide precipitates surrounded by  $\text{Al}_2\text{O}_3$  oxide were found inside  $\text{NiO}$  oxide (Fig. 16). The mass change of the turbine blade aluminized by the VPA method is about  $-4.2 \text{ mg/cm}^2$  after 30 cycles of oxidation.

A continuous and uniform  $\text{Al}_2\text{O}_3$  scale without significant changes was found after 30 cycles of oxidation on the surface of the turbine blade aluminized by the low-activity CVD process (Fig. 17). The topology of the coating shows polygonal grains. The spallation occurs along grain boundaries. The chemical composition of this region corresponds to  $\text{Al}_2\text{O}_3$

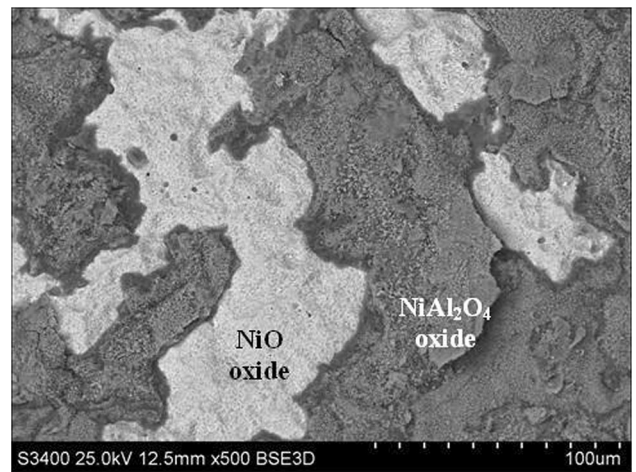


**Fig. 15** SEM micrographs of the oxides formed on the aluminide coating deposited by the VPA method after 30 cycles of oxidation at 1100 °C in the air atmosphere

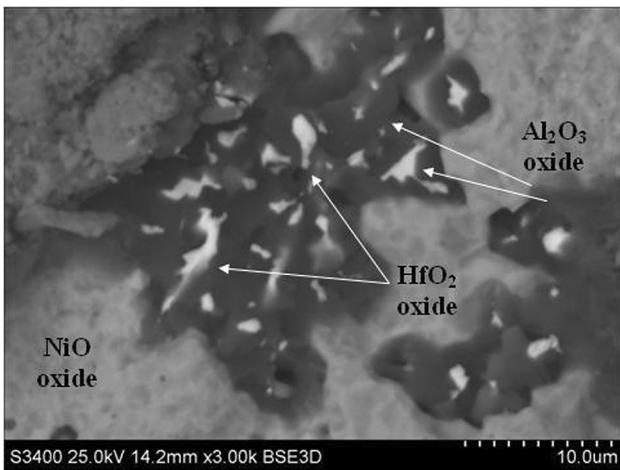


**Fig. 16** SEM micrographs of  $\text{Al}_2\text{O}_3$  and  $\text{HfO}_2$  oxides formed on the aluminide coating deposited by the VPA method after 30 cycles of oxidation at  $1100^\circ\text{C}$  in the air atmosphere



**Fig. 17** SEM micrographs of oxides formed on the aluminide coating deposited by the CVD method after 30 cycles of oxidation at  $1100^\circ\text{C}$  in the air atmosphere

oxide. Some small regions of NiO oxide were also found on the surface of the coating after 30 cycles of oxidation (Fig. 17). The large portion of fine precipitates of  $\text{HfO}_2$  oxide was found on the surface of the coating. Precipitates were distributed both at grain boundaries and inside grains (Fig. 18).

The residual stress measurements were performed after 30 cycles of oxidation. The results are presented in Table 3.

It was found that the residual stress in the aluminide coating after 30 cycles of oxidation at the lock, suction side, and pressure side of the turbine blade was compressive (Table 3). Moreover, the residual stress of the turbine blade after the low-activity CVD aluminizing was more compressive in comparison to the residual stress of the turbine blade after the VPA aluminizing.

#### 4. Discussion

The above experimental results indicate that the aluminide coating deposited by the CVD method protects the turbine

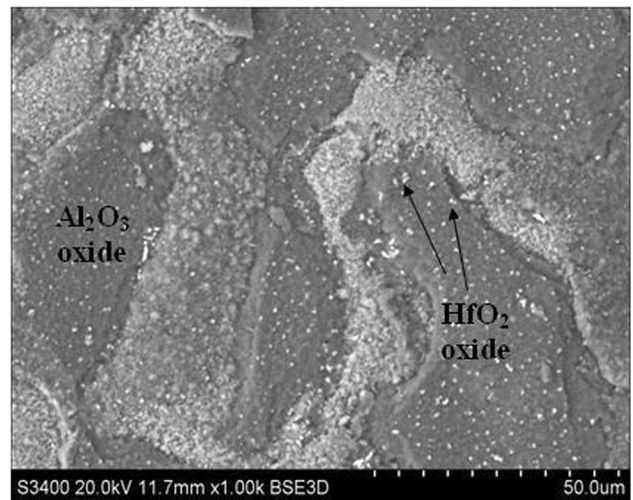


**Fig. 18** SEM micrographs of oxides formed on the aluminide coating deposited by the CVD method after 30 cycles of oxidation at  $1100^\circ\text{C}$  in the air atmosphere:  $\text{Al}_2\text{O}_3$  and  $\text{HfO}_2$  oxides are visible

blade made of ZS6K superalloy up to 50-cycles of oxidation at  $1100^\circ\text{C}$ . Although the aluminide coatings deposited by the VPA method is thicker and the higher aluminum content in the aluminide coating was found in comparison to the coating deposited by the low-activity CVD method, the oxidation resistance of the turbine blade coated in the low-activity process was about seven times higher than the turbine blade coated by the VPA method. Warnes et al. (Ref 16) state that in the VPA process the aluminum source (Al-Cr alloy) contains a large sulfur concentration (about 22 ppm). Sulfur could react with hydrogen in either the pack or the aluminizing process to form the hydrogen sulfide gas. Sulfur (as  $\text{H}_2\text{S}$ ) is transported from the aluminum source (Al-Cr alloy) to the coating. The low-activity CVD aluminizing process takes place without the aluminum source (Al-Cr alloy). The surface is reduced by hydrogen before the aluminizing process. The hydrogen reduction removes sulfur from the surface. Therefore, there is less sulfur than in the coating deposited by the VPA process. The oxidation resistance and the purity of the aluminide coating are related. The removal of impurities from the coating by reactions with hydrogen chloride in the low-activity CVD process produces a “clean” additive layer. Pure aluminide coatings may form a ‘cleaner’ alumina scale that grows slower and is more resistant to oxidation.

It was found that the residual stresses in the aluminide coating deposited by the CVD method were more tensile than in the coating deposited by the VPA method. The different kind of stresses may be associated to different microstructures of coatings after aluminizing processes and different content of impurities. The XRD results indicate the presence of the NiAl phase and MC,  $\text{M}_{23}\text{C}_6$  carbides in the coating deposited in the VPA process. While the XRD results indicate the presence of the NiAl phase in the coating deposited in the CVD process. Moreover, the literature data (Ref 16) report that aluminide coating deposited in the low-activity CVD process has less impurities than the coating deposited in the VPA process. The presence of the NiAl phase, MC and  $\text{M}_{23}\text{C}_6$  carbides in the microstructure of the coating may lead to the increase of the volume of the coating and the decrease of the value of the tensile stresses.



**Table 3 XRD residual stress results after the aluminizing process and 30 cycles of oxidation**

Coating type	Place of stress measurement on turbine blade	Residual stress, MPa	
		Measurement direction	
		x	y
VPA	Lock	$-57 \pm 18$	$-9 \pm 16$
	Suction side	$-29 \pm 24$	$-14 \pm 16$
	Pressure side	$-16 \pm 21$	$-28 \pm 17$
Low-activity CVD	Lock	$-78 \pm 18$	$-70 \pm 18$
	Suction side	$-90 \pm 27$	$-33 \pm 23$
	Pressure side	$-61 \pm 27$	$-38 \pm 14$

The  $\text{Al}_2\text{O}_3$ ,  $\text{NiAl}_2\text{O}_4$  phases, and Hf-rich pegs inside  $\text{Al}_2\text{O}_3$  oxides were found after 10 cycles of oxidation of the aluminide coating deposited by the VPA process. The formation of ‘pegs’ is apparently due to the difference of oxygen diffusivity in  $\text{HfO}_2$  and  $\text{Al}_2\text{O}_3$  scales. The formation mechanism has been proposed as follows:  $\text{Al}_2\text{O}_3$  scales are formed with embedded  $\text{HfO}_2$  particles on hafnium-rich areas, such as grain boundaries (Ref 17, 18). Since the diffusivity of oxygen in  $\text{HfO}_2$  is several orders of magnitude higher than in  $\text{Al}_2\text{O}_3$ ,  $\text{HfO}_2$  particles along Hf-rich grain boundaries act as short circuit diffusion paths for the oxygen transport, leading to preferentially localized scale thickening in the neighborhood of these particles, causing a deep penetration of the formed  $\text{HfO}_2$  scales into the substrate (Ref 17, 18). The oxygen transported through this short circuit diffusion paths reacts with Al atoms in the surrounding areas to form  $\text{Al}_2\text{O}_3$  scales. Therefore  $\text{HfO}_2$  ‘pegs’ surrounded by  $\text{Al}_2\text{O}_3$  are formed.  $\text{NiAl}_2\text{O}_4$  and NiO oxides were found after 30 cycles of oxidation.

The  $\text{Al}_2\text{O}_3$  and  $\text{TiO}_2$  phases were found after 10 cycles of oxidation of aluminide coating deposited by the low-activity CVD process. According to Vialas (Ref 19),  $\text{HfO}_2$  oxide can also be visible on the surface of the aluminide coating after oxidation.  $\text{TiO}_2$  oxide probably grew by the fast Ti diffusion from the substrate to the external oxide surface where it can form  $\text{TiO}_2$  above the existing alumina scale. When an oxide forms at the metal/oxide interface, the volume changes because of the oxide formation. Pilling and Bedworth ratio (Ref 19) of  $\text{Al}_2\text{O}_3$  and  $\text{TiO}_2$  grown on the NiAl phase can be calculated basing on the corresponding molar volumes. It was found that PBR ( $\text{Al}_2\text{O}_3/\text{NiAl}$ ) = 1.8 and PBR ( $\text{TiO}_2/\text{NiAl}$ ) = 2.6. This huge difference means that  $\text{TiO}_2$  growth on the surface of the oxidized coating should cause large local compressive stresses in the oxide scale. These stresses add to the compressive thermal stress during cooling may promote local cracking or spallation.  $\text{Al}_2\text{O}_3$  oxide remains after 30 cycles of oxidation.

The oxidation of the coatings involves the following steps: initial development of the continuous  $\text{Al}_2\text{O}_3$  scale and its propagation inwards and scale spallation with subsequent formation of poorly-protective oxides containing Ni. The next step results in the rapid scale growth and increases the tendency to spallation. After just 10 cycles of oxidation,  $\text{NiAl}_2\text{O}_4$  spinel appears on the surface of the VPA aluminide coating, which in turn spalls easily producing further catastrophic oxidation. Scale spallation of the aluminide coating deposited by the low-activity CVD method starts along grain boundaries. The scales on the grain boundaries contain larger amounts of substrate elements than within the grains. The difference in composition between boundaries and grains may induce higher stress concentrations and yield earlier spalling at these points, especially as a result of mismatch of thermal stresses during

cooling. The residual stresses after aluminizing and 30 cycles of oxidation by both VPA and CVD process were compressive. Moreover, more compressive residual stresses were found in oxides formed on the surface of the aluminide coating deposited by the low-activity CVD process after 30 cycles of oxidation and  $\text{Al}_2\text{O}_3$  protective oxide remained.

## 5. Conclusions

Aluminizing of the turbine blade by means of VPA and CVD methods lead to the formation of two layers (additive and interdiffusion) of the aluminide coatings. The additive and the interdiffusion layers obtained by the VPA method consists of the NiAl phase and some carbides, while the additive layer deposited by the CVD method consist of the NiAl phase only. It was found that residual stresses in the aluminide coating at the lock, suction side, and pressure side of the blade were tensile. The investigation of oxidation resistance revealed that the aluminide coating deposited by the CVD method is about 7 times better than that deposited by the VPA method.  $\text{Al}_2\text{O}_3 + \text{HfO}_2 + \text{NiAl}_2\text{O}_4$  phases were revealed on the surface of the aluminide coating deposited by the VPA method after 240 h oxidation. Meanwhile  $\text{Al}_2\text{O}_3 + \text{TiO}_2$  oxides were found on the surface of aluminide coating deposited by the CVD method after 240 h oxidation. Increasing the time of oxidation from 240 to 720 h led to the formation of the NiO oxide on the surface of the coating deposited by the VPA method.  $\text{Al}_2\text{O}_3$  oxide is still visible on the surface of the coating deposited by the CVD method. The residual stresses in the aluminide coating after 30 cycles of oxidation at the lock, suction side, and pressure side of the turbine blade are compressive.

## Open Access

This article is distributed under the terms of the Creative Commons Attribution 4.0 International License (<http://creativecommons.org/licenses/by/4.0/>), which permits unrestricted use, distribution, and reproduction in any medium, provided you give appropriate credit to the original author(s) and the source, provide a link to the Creative Commons license, and indicate if changes were made.

## References

1. Q. Wu, R. Yang, Y. Wu, S. Li, Y. Ma, and S. Gong, A Comparative Study of Four Modified Al Coatings on  $\text{Ni}_3\text{Al}$ -Based Single Crystal Superalloy, *Prog. Nat. Sci.*, 2011, **21**, p 496–505

2. L. Swadźba, A. Maciejny, and B. Formanek, Microstructure and Resistance to Cracking of Modified Al-Si and AlCr Diffusion Coatings on ZS6K Nickel-Based Superalloys, *Surf. Coating Technol.*, 1992, **54**(55), p 84–90
3. G.W. Goward and D.H. Bone, Mechanisms of Formation of Diffusion Aluminide Coatings on Nickel-Base Superalloys, *Oxid. Met.*, 1971, **3**(5), p 50–55
4. M. Pytel, M. Góral, M. Motyka, and T. Miziniak, Thermal Stability of Protective Coatings Produced on Nickel Based Superalloy, *J. Achiev. Mater. Manuf. Eng.*, 2012, **51**, p 67–77
5. W. Sun, H.J. Lin, and M. Hon, CVD Aluminide Nickel, *Metallurgical and Materials Transactions A*, 1986, **17**(2), p 215–220
6. S. Bose, *High Temperature Coatings*, Elsevier, Burlington, 2007
7. M. Zielińska, M. Zagula-Yavorska, J. Sieniawski, and R. Filip, Microstructure and Oxidation Resistance of an Aluminide Coating on the Nickel Based Superalloy Mar M247 Deposited by the CVD Aluminizing Process, *Arch. Metall. Mater.*, 2013, **58**, p 697–701
8. M. Watanabe, D. Mumm, S. Chiras, and A. Evans, Measurement of the Residual Stress in a Pt-Aluminide Bond Coat, *Scripta Mater.*, 2002, **46**, p 67–70
9. J. Romanowska, M. Zagula-Yavorska, and J. Sieniawski, Zirconium Influence on Microstructure of Aluminide Coatings Deposited on Nickel Substrate by CVD Method, *Bull. Mater. Sci.*, 2013, **36**, p 1043–1048
10. J. Romanowska, Aluminum Diffusion in Aluminide Coatings Deposited by the CVD Method on Pure Nickel, *CALPHAD*, 2014, **44**, p 114–118
11. M. Zagula-Yavorska, J. Sieniawski, and T. Gancarczyk, Some Properties of Platinum and Palladium Modified Aluminide Coatings Deposited by CVD Method on Nickel-Base Superalloys, *Arch. Metall. Mater.*, 2012, **57**, p 503–509
12. A. Ginnis, T. Watkins, and K. Jagannadham, Residual stresses in a multilayer system of coatings, *JCPDS Int. Centre Diffr. Data*, 1999, pp. 443–454
13. L.C. Noyan and J.B. Cohen, *Residual Stress: Measurement by Diffraction and Interpretation*, Vol 120–126, Springer, New York, 1987, p 223–229
14. E.H. Chung and D.K. Smith, *Industrial Applications of X-Ray Diffraction*, Marcel Dekker, New York, 2000
15. S. Prevey, *X-Ray Diffraction Residual Stress Techniques, Metals Handbook*, Vol 10, 9th ed., American Society for Metals, Metals Park, 1986, p 380–392
16. B. Warnes and D. Punola, Clean Diffusion Coatings by Chemical Vapor Deposition, *Surf. Coat. Technol.*, 1997, **94–95**, p 1–6
17. Y. Wang and M. Suneson, Synthesis of Hf-Modified Aluminide Coatings on Ni-Base Superalloys, *Surf. Coat. Technol.*, 2011, **206**, p 1218–1228
18. H. Hindam and D.P. Whittle, Microstructure, Adhesion and Growth Kinetics of Protective Scales on Metals and Alloys, *J. Electrochem. Soc.*, 1982, **5**(6), p 245–284
19. N. Vialas and D. Monceau, Substrate Effect on the High-Temperature Oxidation Behavior of a Pt-Modified Aluminide Coating. Part I: Influence of the Initial Chemical Composition of the Coating Surface, *Oxid. Met.*, 2006, **66**, p 155–189